



A 30 m soil and water conservation terrace measures dataset of China from 2000 to 2020

Enwei Zhang¹, Yueli Chen³, Shengzhao Wei¹, Chenli Liu¹, Hongna Wang¹, Bowen Deng¹, Honghong Lin¹, Xue Yang¹, Yawen Li¹, Xingwu Duan^{1,2,*}

5 ¹Yunnan Key Laboratory of Soil Erosion Prevention and Green Development, Institute of International Rivers and Eco-Security, Yunnan University, Kunming, 650500, China

²State Key Laboratory for Vegetation Structure, Function and Construction, Yunnan University, Kunming, 650500, China

³State Key Laboratory of Severe Weather Meteorological Science and Technology, Chinese Academy of Meteorological Sciences, Beijing, 100081, China

10 *Correspondence to:* Xingwu Duan (xwduan@ynu.edu.cn)

Abstract. Terrace, as one of the most widely distributed and heavily invested soil and water conservation (SWC) measures in China, currently lacks a comprehensive database with spatiotemporal distribution and diverse classification types. This absence significantly hampers accurate soil erosion assessment and SWC planning in China. To address this gap, we proposed a two-stage mapping framework for the different terrace measures classification to produce a new dataset named the Soil and Water Conservation Terrace Measures Dataset (SWCTMD) using time-series Landsat satellite imagery and digital elevation model data. This dataset, spanning from 2000 to 2020, incorporated a fine classification system, providing both terrace data and SWC measure factor. The terraces were classified into four types according to their features: level terrace, slope terrace, zig terrace, and slope-separated terrace. The results showed that the average overall accuracy (OA) of the terrace was 91.90% and the average F1 score was 76.75%. For different terrace types, the average OA was 83.50% and the average F1 score was 52.14%. Comparative analysis highlighted the superiority and robustness of the SWCTMD compared to existing products. This dataset revealed that terraces in China are predominantly concentrated in the Loess Plateau, Southwest and Southeast regions. From 2000 to 2020, the total terrace areas increased by 96,038.16 km², with the largest increase occurring in slope terraces. While terrace expansion was concentrated in the Loess Plateau, and southwest and southeast of China, decreases were concentrated around urban areas. Notably, terraces reduced soil erosion of cropland by about 818 million tons in 2020. The SWCTMD enhances the accuracy of soil erosion simulations and enables long-term analysis of soil erosion trends. Moreover, the dataset offers valuable applications in earth system modelling and contributes to research on land resource management, food security, biodiversity, and water cycle. The SWCTMD is freely available at <https://doi.org/10.11888/Terre.tpd.302400> (Duan, 2025).

1 Introduction

30 Agricultural terraces are one of the most common cultivation techniques in mountainous and hilly areas, varying in shape and size. They consist of flat cultivated section and nearly vertical riser. The riser is usually protected by dry stone, grass,



scrub or trees, ranging from a few centimeters to several meters in height and may be continuous or intermittent (Arnáez et al., 2015). As an important soil and water conservation (SWC) measure, terraces have a significant effect on retaining water and soil (Wickama et al., 2014; Londero et al., 2018). Based on the structures of the field surface, terraces can be categorized
35 into level terrace, slope terrace, zig terrace, and slope-separated terrace (Liu et al., 2013a). By reshaping surface microtopography, terraces decreased slope length and gradient and changed specific hydrological paths (Deng et al., 2021). These changes reduce soil erosion and runoff, improve conserving water and soil, and increase crop yields (Adgo et al., 2013; Chen et al., 2017, 2020; Wei et al., 2021). Within established soil erosion assessment frameworks, terraces are shown as a support practice factor in the Universal Soil Loss Equation (USLE) and the Revised Universal Soil Loss Equation (RUSLE)
40 (Wischmeier and Smith, 1978; Renard et al., 1997). In the Chinese Soil Loss Equation (CSLE), they are specifically represented as SWC engineering practice factor (Liu et al., 2020a). However, many large-scale assessments of soil erosion neglect this factor due to insufficient data on the spatial distribution of terraces (Gobin et al., 2004; Teng et al., 2016). Therefore, the mapping of terraces is crucial for soil erosion research.

Efforts have been made to map terraces in China. Three primary methods are employed to obtain the spatial extent and
45 location information of terraces. The first method is government-initiated land resource survey. In the second and third nationwide land survey of China, terraces were considered in paddy field surveys. Terraces located in extensive drylands, particularly on steep slope land, were often categorized simply as dryland or irrigated land, without distinguishing terrace types. The second method is to extract terrace information from land use data (Liu et al., 2021). Existing land use products in
50 China, such as FROM-GLC, GlobeLand30, CLCD, CACD, and GLC_FCS30, generally classify terraces as cropland (Yu et al., 2013; Chen et al., 2015; Yang and Huang, 2021; Zhang et al., 2021; Tu et al., 2024). Among these, only the CNLUCC land use product further subdivides cropland into paddy field and dryland but still fails to distinguish terrace types on dryland (Liu et al., 2010). This limitation makes it challenging to extract terraces from existing land use data. The third method is to use satellite images to identify terraces. For instance, Lu et al. (2023) used deep learning methods to map
55 terraces in the Loess Plateau based on high-resolution satellite images from October 2018 to February 2019. Li et al. (2024) produced a 30-meter resolution terrace map for China using 2017 Sentinel-2 imagery and Landsat-8 imagery on the Google Earth Engine (GEE) platform through the random forest (RF) algorithm. Similarly, Cao et al. (2021) produced a 30-meter resolution terrace map using 2018 Landsat-8 imagery and the RF algorithm on the GEE platform (Table 1). Although these maps have been widely used in soil erosion research (Li et al., 2023; Zhang et al., 2023), the limited classification of terrace types and lack of long-term coverage restrict broader application at regional or national scales. The effectiveness of terraces
60 in SWC varies significantly by type, with level terraces exhibiting the most remarkable benefits (Oliveira et al., 2012). Level terraces reduced runoff by 56.5% and sediment by 53.1% compared to slope terraces (Chen et al., 2017). Ignoring terrace types can lead to inaccuracies in soil erosion assessment. Furthermore, the absence of long-term terrace data hinders analyses of soil erosion trends and predictions.



Table 1. Existing terrace products in China.

Method	Algorithm	Study area	Data	Reference
Deep learning	Mapping terraces based on UNET++ deep learning network	The Loess Plateau	Google Earth images	Lu et al. (2023)
Machine learning	Mapping terraces based on RF algorithm	China	Landsat-8 imagery and Sentinel-2 imagery	Li et al. (2024)
Machine learning	Mapping terraces based on RF algorithm	China	Landsat-8 imagery	Cao et al. (2021)

70 Steep slope land accounts for more than one-third of the total cropland area in China. Over recent decades, the construction of agricultural terraces has been the primary engineering measure for managing steep slope cropland (Liu et al., 2013b; Feng et al., 2017; Zhang et al., 2017). However, the existing terrace datasets lack detailed classification of terrace types and are limited to single-year data. These limitations hinder soil erosion assessment, prediction, and SWC planning. To address this gap, a two-stage mapping framework for the terrace classification was developed on the GEE platform. The first stage distinguishes terraces from non-terraces, while the second stage focuses on identifying different terrace types. Using this mapping framework, the first Soil and Water Conservation Terrace Measures Dataset of China (SWCTMD) was produced
75 using time-series Landsat satellite imagery and digital elevation model data, covering the period from 2000 to 2020. The dataset incorporates a detailed classification system. The accuracy of SWCTMD was evaluated using validation samples and compared with existing terrace maps. Additionally, the terrace dataset was used to identify spatial and temporal changes in terraces across China and to assess the SWC benefits provided by terraces.

2 Methodology

80 Figure 1 illustrates the framework of terrace mapping, which includes sample collection, feature calculation, classification implementation, post-classification processing, and accuracy evaluation. Detailed information on each stage of the terrace mapping process is provided below.

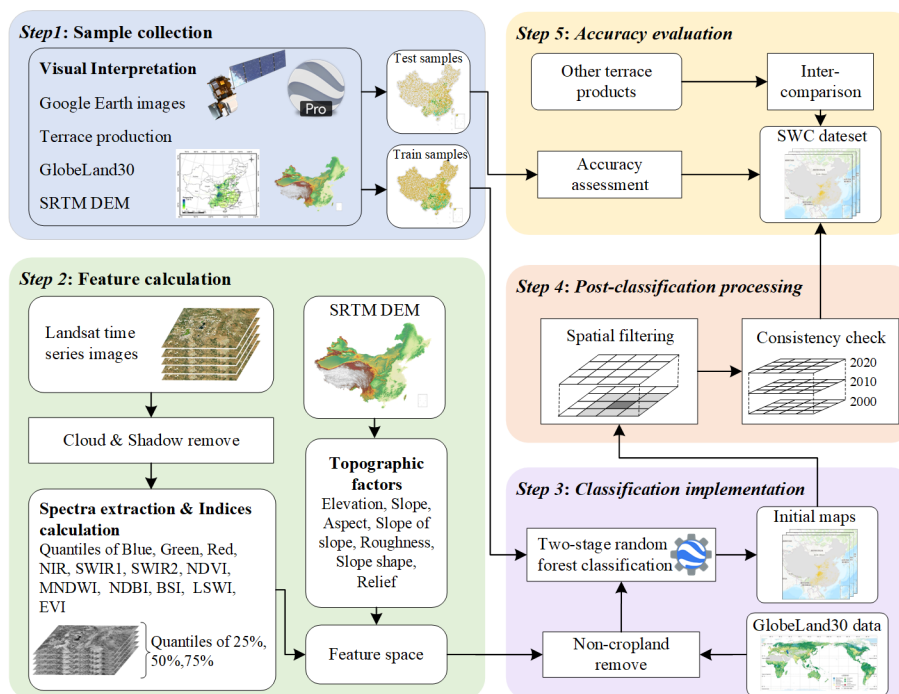


Figure 1. The framework for mapping terrace.

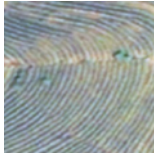
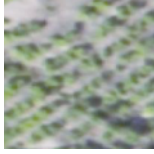
85 2.1 The classification system and interpretation symbols

According to the findings of China’s First National Census for Water (FNCW) (Liu et al., 2020a), we identified the major types of terraces, including level terrace, slope terrace, zig terrace, and slope-separated terrace. The interpretation keys for the different terrace types included shape, size, texture, color, and location (Table 2).

Table 2. Image characteristics of different terrace types.

Terrace types	Image characteristics	Remote sensing image
Level terrace	Steep slope land transformed into a series of successively receding flat surfaces, with bunds constructed from soil or stones, ranging in width from 5 to 40 m, looking like the steps of a staircase in remote sensing images. In contrast to slope terraces, level terraces are predominantly found in low and flat areas.	
Slope terrace	Similar to level terraces, but with wider and more uneven surfaces, these terraces exhibit irregular shapes in remote sensing images. They are primarily used for dryland agriculture and are mostly distributed the areas with slopes greater than 5°.	



Zig terrace	Steep slope land has been transformed into step-like terraces, which are narrower than level terraces. The surfaces of these terraces exhibit regular strip shapes in remote sensing images. These terraces are primarily found in sloping regions and are used for planting permanent crops such as tea.	
Slope-separated terrace	Each flat surface constructed on steep slope land retains an original slope segment above it, forming a composite structure that features a slope between flat surfaces. These terraces are primarily used for rubber plantations.	

90 2.2 Data and preprocessing

In this study, we primarily used Landsat surface reflectance (SR) data, Shuttle Radar Topography Mission (SRTM) digital elevation model (DEM) data, and GlobeLand30. Detailed information about these datasets is provided in Table S1.

2.2.1 Landsat SR data

95 The study used Landsat-4/5/7/8 SR data, with a spatial resolution of 30 m and a temporal resolution of 16d, which were accessible through the GEE platform. The Landsat SR data from all the sensors have been atmospherically corrected by the United States Geological Survey (USGS) utilizing the LEDAPS algorithm (Masek et al., 2006). These data included Quality Assessment (QA) masks that indicated the usability of the pixel data, produced using the CFMASK algorithm (Zhu and Woodcock, 2012). We used QA bands to identify and remove clouds and cloud shadows in each Landsat SR image, and the missing data within the year after cloud removal was filled using images from the previous year. Due to the inconsistency in
100 the wavelength of band among different Landsat sensors (Roy et al., 2016), we used only Landsat-8 SR imagery for the SWCTMD in 2020, and Landsat-4/5/7 SR imagery for the SWCTMD in 2000. In 2010, we relied solely on Landsat-5 SR imagery for the SWCTMD due to the failure of the Scan Line Corrector in the Landsat-7 instrument in 2003 and the decommissioning of Landsat-4 in 2001.

2.2.2 SRTM DEM

105 Topographical features are essential characteristics that differentiate regular cropland and terrace, playing a crucial role in the identification of terraces. We used the SRTM DEM data to calculate these topographical features. SRTM is a global research effort that acquired DEM with near-global coverage, achieving a resolution of 1 arcsecond. The SRTM DEM has been processed for void-filling utilizing various open-source DEM datasets. Compared to other DEM data, SRTM DEM is the most quality-controlled, broadest coverage, and highest accuracy DEM among open-source data (Farr et al., 2007; Dong
110 et al., 2015). The GEE platform provides access to the SRTM DEM at 30 m resolution.



2.2.3 GlobeLand30

To improve the accuracy and efficiency of terrace identification, we use the union of cropland data from GlobeLand30 from 2000 to 2020 as the range of terrace identification. GlobeLand30 is a widely global used land use dataset that adopts a pixel-object-knowledge classification method, effectively utilizing the advantages of various classification algorithms (Chen et al., 2015). The accuracy of cropland area and spatial location of GlobeLand30 is higher than the other four products (FROM-GLC, GlobCover, MODIS Collection 5, and MODIS Cropland) in China (Lu et al., 2016). The cropland from GlobeLand30 includes paddy fields, drylands, pastures, and permanent crop lands (such as tea and coffee). Therefore, we adopt the cropland from GlobeLand30 as the range of terrace classification.

2.3 Feature space construction

Feature variables play a crucial role in remote sensing image classification. In this study, we constructed an input dataset comprising five aspects: spectrum, spectral indices, phenology, texture, and topography. The six optical bands (red, green, blue, near-infrared, shortwave infrared 1, and shortwave infrared 2) from Landsat SR imagery for a specific year, along with the corresponding spectral indices (NDVI, MNDWI, NDBI, BSI, LSWI, and EVI), were composited into the 25th, 50th, and 75th percentiles utilizing the metrics-composite method. The percentiles effectively represent phenological information while simplifying time series information, reducing annual time series noise, and contributing to enhanced classification accuracy (Duan et al., 2024). Additionally, texture features can notably improve classification precision (Liu et al., 2020b; Maskell et al., 2021; Duan et al., 2022). Due to the high similarity among the six optical bands of Landsat SR imagery, only the texture features of the near-infrared band were considered in this study (Rodriguez-Galiano et al., 2012a; Zhang et al., 2021). Furthermore, to avoid redundancy among texture features, four texture features of the infrared band, including Angular Second Moment (ASM), Entropy, Contrast, and Correlation, were selected (Hou et al., 2013). In addition to the Landsat-based metrics, we incorporated seven frequently utilized topographic features, including slope, aspect, slope of slope, relief, slope shape, roughness, and elevation (Tang et al., 2016). In total, we acquired 55 features for each year (Table S2).

2.4 Training and validation sample collection

Samples are a critical component in supervised classification. We used manual visual interpretation methods to collect samples in the years 2000, 2010, and 2020. To ensure that the collected samples are evenly distributed across the study area, we implemented a strategy of gathering samples by subregions. The study area was divided into 1,641 subregions. Utilizing high-resolution images from Google Earth Pro software, we collected at least 10 samples from each subregion (Fig. 2). Through this method, we collected a total of 52,329 samples. Specifically, a total of 17,392 samples were collected in 2000, 17,417 samples in 2010, and 17,520 samples in 2020 (Table S3). Subsequently, we split the annual samples into training (70%) and validation data (30%) (Figs. S1 and S2).

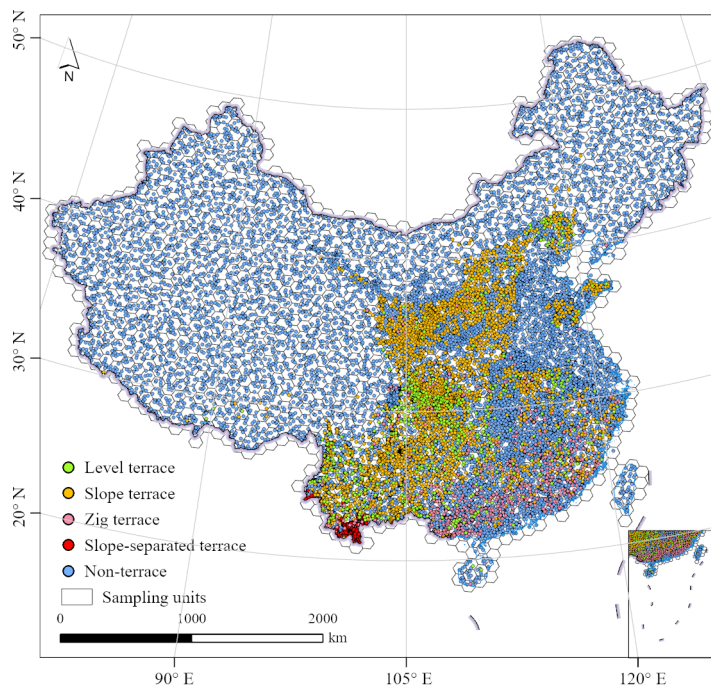


Figure 2. The spatial distribution of samples in 2010.

2.5 Terrace classification on the GEE platform

145 The GEE platform offers a variety of classification algorithms. We select the widely used RF model for terrace classification, given the algorithm has the advantages of remarkable performance, high efficiency, and interpretability (Rodriguez-Galiano et al., 2012b; Gong et al., 2019). Two essential parameters must be set for the RF model. In this study, we set the number of trees to 500 and determined the number of variables per split as the rounded square root of the feature number. Other parameters were maintained at their default settings as specified by the GEE platform (He et al., 2017; Gong et al., 2020).

150 Given the sensitivity of the RF model to the ratio of samples across different classes (Chen et al., 2024), we implemented a two-stage mapping approach for classifying terraces. In the first stage, RF was utilized to differentiate between terrace and non-terrace classes. In the second stage, RF was utilized to classify various terrace types, including level terrace, slope terrace, zig terrace, and slope-separated terrace. In Stage I of the mapping process, samples from both terrace and non-terrace samples were used, whereas only terrace samples were utilized in Stage II.

155 2.6 Post-classification processing

Both supervised and unsupervised classification methods in remote sensing rely on the spectral characteristics of image pixels. A critical issue is the presence of isolated pixels in the classification results, which exhibit high local spatial heterogeneity between neighboring pixels (Hirayama et al., 2019). This phenomenon, commonly known as the salt-and-pepper effect, is regarded as noise affecting accuracy. Terraces, primarily constructed in hilly or mountainous regions,



160 exhibit a scattered and irregular distribution, which leads to an obvious salt-and-pepper effect in classified images. Given the
small area of terraces, we applied a mode filter with 3×3 px for spatial filtering processing to mitigate the salt-and-pepper
effect from the classification results. To improve the overall quality of the mapping results, we conducted spatial-temporal
consistency check to suppress illogical land use conversions. Specifically, for areas that were cropland in both the previous
year and the current year (excluding grain-for-green areas), we modified those areas that were previously terraces but were
165 identified as non-terraces in the current year to terraces.

2.7 Accuracy assessment

It is an essential step to assess the accuracy of the products prior to utilizing data in related applications. The classification
maps were evaluated using a confusion matrix calculated from validation samples. The confusion matrix is widely regarded
as the standard method for evaluating the accuracy of classified images. This method offers quantitative assessment metrics,
170 including the kappa coefficient (KA), overall accuracy (OA), producer's accuracy (PA), and user's accuracy (UA), which
collectively assess the performance of the products. In addition, we calculated the F1 score, which reflects the balance
between UA and PA. The formula is Eq. (1):

$$F1 = 2 \frac{PA \times UA}{(PA + UA)} \quad (1)$$

175 In this study, we constructed two confusion matrices: one for evaluating the accuracy of terraces and non-terraces, and the
other for assessing the accuracy of various terrace types.

3 Results

3.1 Accuracy assessment of the dataset

Using the validation samples, two confusion matrices corresponding to different terrace classification levels were generated.
180 For the classification of terrace and non-terrace, the OA ranged from 90.44% to 92.89%, with KA ranging from 64.83% to
76.75%, and F1-scores ranging from 70.14% to 95.62% (Table 3), indicating that the classification performs well. For
terrace class, the UA ranged from 87.83% to 92.09%, and the PA ranged from 56.64% to 75.32%, indicating that the
probability of misclassification for terrace was low.

Table 3. The accuracy matrix for the terrace and non-terrace.

Year	types	UA (%)	PA (%)	F1 score (%)	OA (%)	Kappa (%)
2000	Non-terrace	90.21	98.80	94.31	90.44	64.83
	Terrace	92.09	56.64	70.14		
2010	Non-terrace	92.61	98.22	95.33	92.37	74.45



	Terrace	91.06	69.79	79.02		
2020	Non-terrace	93.95	97.35	95.62	92.89	76.75
	Terrace	87.83	75.32	81.09		

185

For different terrace types, the OA ranged from 81.31% to 86.03%, KA ranged from 37.37% to 50.01%, and F1 scores ranged from 22.86% to 92.27% (Table 4). Slope terraces exhibited the highest classification accuracy, followed by slope-separated terraces, level terraces, and zig terraces, respectively. From the UA and PA, the omission errors were lower than the commission errors for different types of terraces. Among all terrace types, slope terrace had the lowest misclassification error.

190

Table 4. The accuracy matrix for the different types of terraces.

Year	types	UA (%)	PA (%)	F1 score (%)	OA (%)	Kappa (%)
2000	Level terrace	66.67	18.18	28.57	81.31	37.74
	Slope terrace	84.03	97.98	90.47		
	Zig terrace	44.44	15.38	22.86		
	Slope-separated terrace	57.14	35.82	44.04		
2010	Level terrace	90.00	22.50	36.00	83.15	37.37
	Slope terrace	84.08	98.26	90.62		
	Zig terrace	62.50	15.15	24.39		
	Slope-separated terrace	63.33	45.24	52.78		
2020	Level terrace	77.27	24.64	37.36	86.03	50.01
	Slope terrace	87.00	98.23	92.27		
	Zig terrace	41.18	18.42	25.45		
	Slope-separated terrace	92.68	71.70	80.85		

195

We compared the 2020 terraces in the SWCTMD with two existing terrace data, the 2018 terrace map (Cao et al., 2021) and the 2017 terrace map (Li et al., 2024), finding that our results exhibit higher accuracy and robustness. Their research primarily focused on terraces found in paddy fields and drylands, whereas our research covers a broader range, including slope-separated terraces constructed in rubber plantation regions and zig terraces in orchard lands in southern China. Notably, we identified massive zig terraces such as Guangxi, where the terraces mapped by Cao and Li are relatively sparse (Fig. 3). This discrepancy indicates that our datasets offer more comprehensive coverage for recognizing terraces. Despite the 2 to 3-year temporal gap between the datasets, the changes in terraces during this period were minimal, suggesting that the temporal disparity does not affect the comparative result.

200

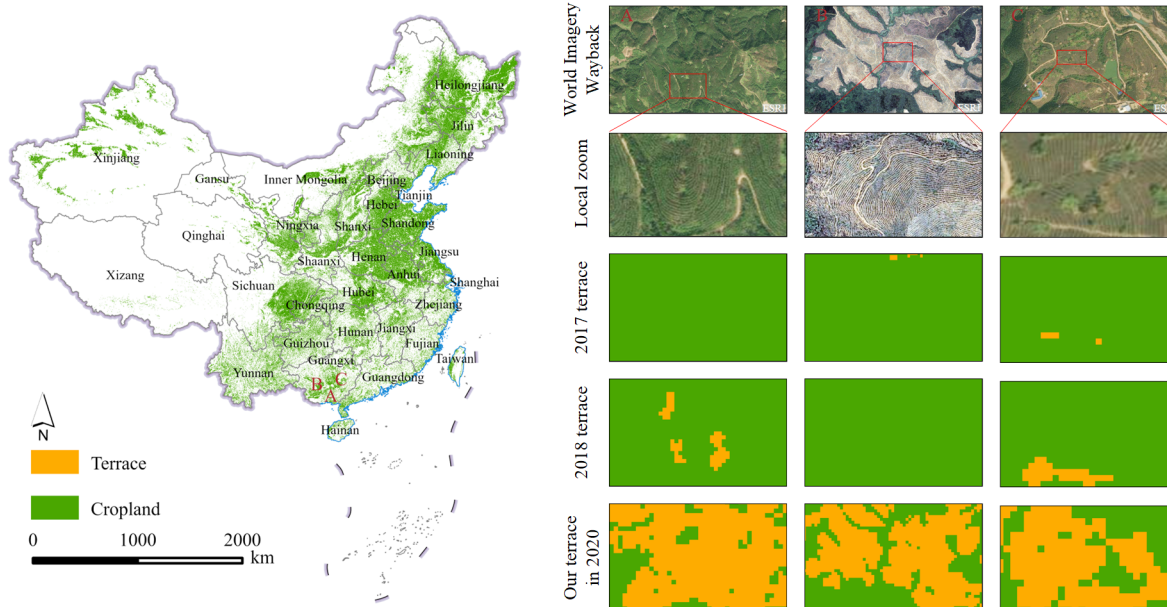


Figure 3. Regional comparisons of the three terraces data.

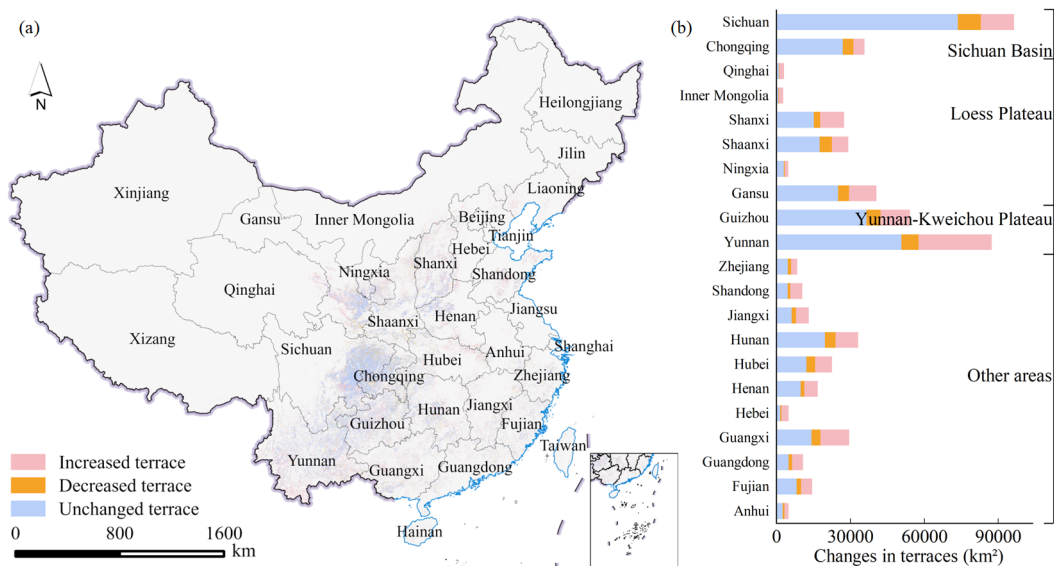
3.2 Spatiotemporal variation of terraces in China

Terraces are primarily distributed across the hills, basins, and plateaus of China (Figs. 4a and S3). The Sichuan Basin exhibits the highest concentration of terraces, followed by the Yunnan-Kweichou Plateau and the Loess Plateau. Furthermore, terraces are also extensively found in the hilly regions of central and southeastern China. From terrace types, level terraces are distributed in the gentler slopes of hilly regions in southern China. Sloped terraces are most extensively distributed across the Sichuan Basin, Yunnan-Kweichou Plateau, and Loess Plateau, with smaller occurrences in the hilly regions of central and southeastern China. Zig terraces are mostly distributed in the central and southeastern hilly areas, while slope-separated terraces are mainly located in southwest China (Figs. 4a and 4b). In terms of spatial changes, the increasing terraces are mainly distributed in the Yunnan-Kweichou Plateau, Loess Plateau, and Sichuan Basin from 2000 to 2020 (Fig. 5a). These areas are severely affected by soil erosion and are key areas of soil erosion in China. Yunnan and Gansu are the provinces with the largest increase in terraces (Fig. 5b). The decreasing terraces are mainly distributed around urban areas from 2000 to 2020, where urban expansion has occupied some terrace areas.



215

Figure 4. The spatial patterns of different terrace types at pixel and provincial. (a) The spatial distribution of different terraces in China in 2020. (b) The different terrace areas in different provinces in 2020.



220

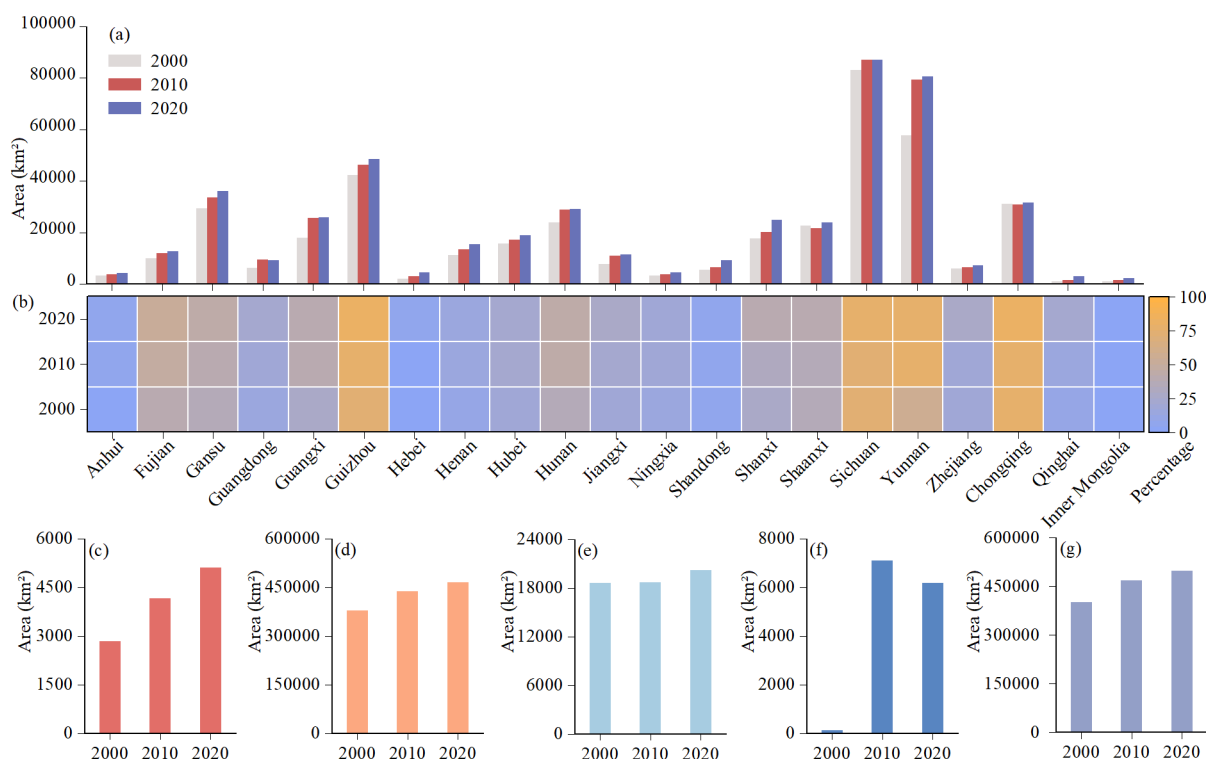
Figure 5. The spatial changes of the terrace at pixel and provincial. (a) The spatial changes in terraces from 2000 to 2020. (b) The changes in the terrace areas in different provinces from 2000 to 2020.

The provinces with the largest terrace areas are Sichuan, Yunnan, Guizhou, Gansu, and Chongqing, while other provinces have relatively smaller terrace areas (Fig. 6a). Among these, Chongqing, Sichuan, Guizhou, and Yunnan exhibited the highest percentage of terraces, with over 70% of cropland converted to terraces (Fig. 6b). From 2000 to 2020, Yunnan, Gansu, Guangxi, and Guizhou experienced the most significant increases in terrace areas, with the terrace areas increasing by 22,877.35 km², 6,822.40 km², 8,095.66 km², and 6,235.54 km², respectively (Fig. 6a). In terms of terrace types, the areas

225



of level terraces, slope terraces, zig terraces and slope separated terraces increased by 2,275.26 km², 86,186.26 km², 1,536.28 km², and 6,040.36 km², respectively, with the slope terrace having the largest increasing areas (Figs. 6c, d, e and f). Overall, China's total terrace area expanded from 400,895.68 km² in 2000 to 496,933.84 km² in 2020 (Fig. 6g).



230 **Figure 6.** The changes of terrace areas at provincial and types from 2000 to 2020. (a) The changes of terrace area in different provinces. (b)
 The proportion of terraces to cropland in different provinces. (c-f) The areas of level terrace, slope terrace, zig terrace, and slope-separated
 235 terrace, respectively. (g) The total terrace areas of China.

3.3 Spatiotemporal pattern of E in China

The SWC engineering practices indicate the ratio of the amount of soil erosion with specific measures to the corresponding
 235 amount without measures, denoted by E. The values of E range from 0 to 1, with lower values showing better SWC benefits.
 We generated spatial distribution maps of E values based on the SWCTMD for the years 2000, 2010, and 2020 (Fig. 7). The
 E values for different terrace types were determined based on existing studies (Duan et al., 2020; Liu et al., 2020a). The
 measures with the worst SWC benefit were mainly distributed in southwest China. The measures with the best SWC benefit
 were scattered in the gentler slopes of among hills, and southeastern China. Overall, the Yunnan-Kweichou Plateau, the
 240 Sichuan Basin, and the Loess Plateau exhibited the best performance for SWC (Figs. 7a, b and c).

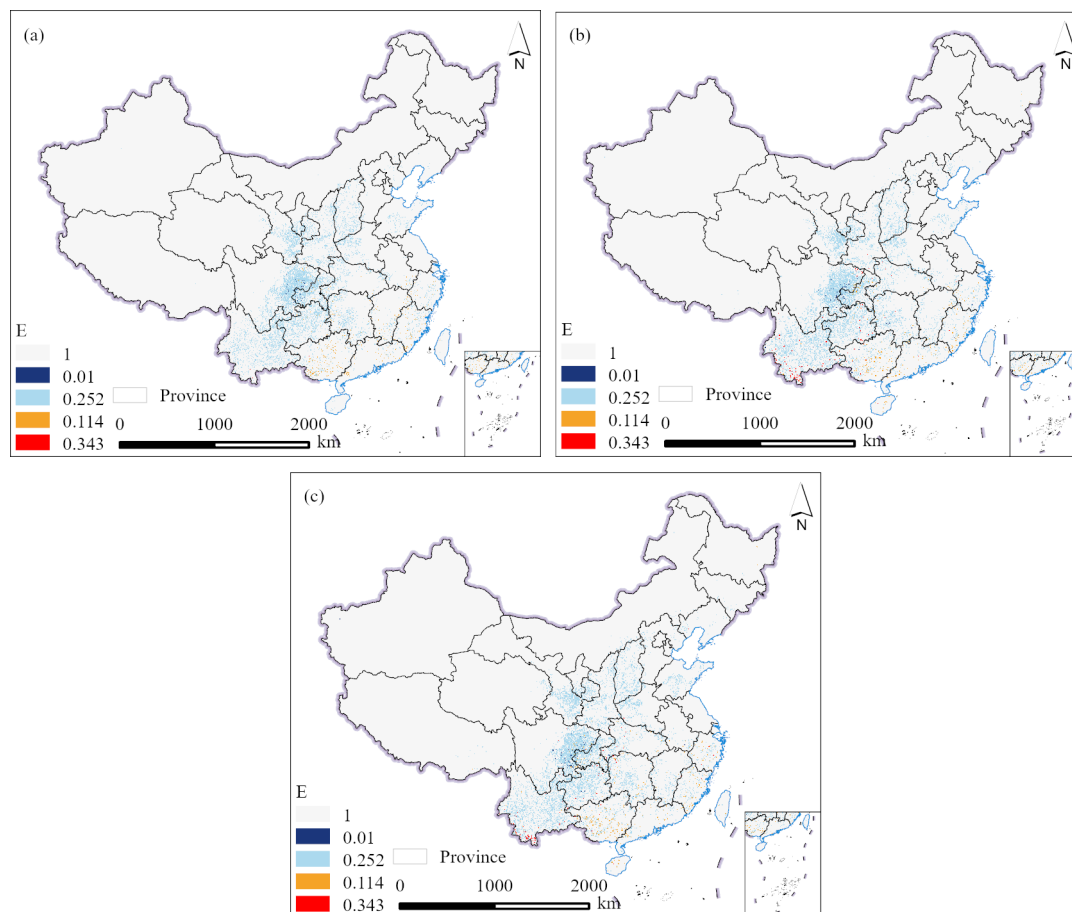


Figure 7. Spatial variances of the value of E. (a-c) Spatial variation of E value in 2000, 2010, and 2020, respectively.

3.4 Responses of soil erosion to terraces in China

We utilized the CSLE to assess the soil erosion modulus of cropland in China for the year 2020 using the SWCTMD (Note
245 S1). The soil erosion area was calculated according to the standards for classification and gradation of soil erosion (Note S2).
Figure 8 illustrates the soil erosion modulus under a terrace scenario in 2020. The average soil erosion modulus for cropland
was $10.82 \text{ t}\cdot\text{ha}^{-1}\cdot\text{y}^{-1}$, with a total eroded area is $1,010,986.69 \text{ km}^2$. The impact of terraces on soil erosion was assessed by the
differences between scenarios with and without terraces. Compared to the scenario without terrace measures, the average soil
erosion modulus of cropland decreased by $4.18 \text{ t}\cdot\text{ha}^{-1}\cdot\text{y}^{-1}$, and the erosion area was reduced by $54,833.06 \text{ km}^2$ (Figs. S4a and
250 b). In terms of spatial distribution, the Yunnan-Kweichou Plateau, Sichuan Basin, and Loess Plateau exhibit the most
significant reduction in soil erosion. The reductions in soil erosion modulus for Chongqing, Sichuan, Guizhou, Yunnan,
Shanxi, Gansu, and Shaanxi were $22.83 \text{ t}\cdot\text{ha}^{-1}\cdot\text{y}^{-1}$, $21.31 \text{ t}\cdot\text{ha}^{-1}\cdot\text{y}^{-1}$, $18.64 \text{ t}\cdot\text{ha}^{-1}\cdot\text{y}^{-1}$, $14.61 \text{ t}\cdot\text{ha}^{-1}\cdot\text{y}^{-1}$, $6.48 \text{ t}\cdot\text{ha}^{-1}\cdot\text{y}^{-1}$, $4.52 \text{ t}\cdot\text{ha}^{-1}\cdot\text{y}^{-1}$,
 $3.81 \text{ t}\cdot\text{ha}^{-1}\cdot\text{y}^{-1}$, respectively, with corresponding reductions in erosion area of $3,702.75 \text{ km}^2$, $12,774.31 \text{ km}^2$, $4,023.94$
 km^2 , $7,169.19 \text{ km}^2$, $2,515.31 \text{ km}^2$, $6,108.56 \text{ km}^2$, and $2,980.56 \text{ km}^2$ (Fig. 8a). According to our estimation, the terrace



255 measures reduced approximately 818 million tons of soil erosion on cropland, accounting for 37.61% of the total erosion on cropland. In comparison to the scenario without terrace measures, the amount of soil erosion in the regions of Yunnan, Sichuan, Chongqing, Guizhou, Gansu, Shanxi, and Shaanxi regions decreased by 47.47%, 46.02%, 45.57%, 45.25%, 35.48%, 29.75%, and 27.80%, respectively (Fig. 8b). In contrast, other regions had fewer SWC measures, and the difference in soil erosion with and without measures was small.

260

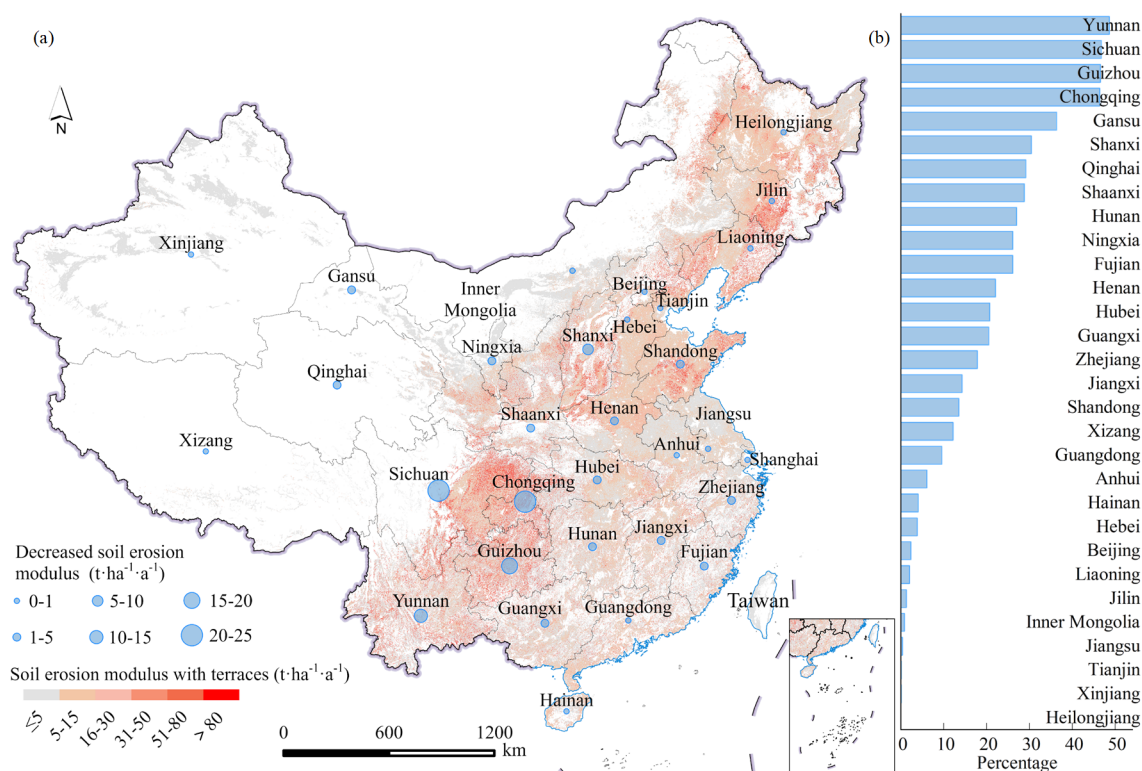


Figure 8. The effects of terraces on soil erosion in different provinces. (a) The soil erosion is alleviated by terraces. (b) The percentage represents the amount of soil erosion alleviated by terraces as a proportion of the total soil erosion without terraces.

265 4 Discussion

4.1 Spatial pattern of terraces

The Sichuan Basin, Loess Plateau, and the Yunnan-Kweichou Plateau are the three regions with the highest concentration of terraces in China. Other areas, characterized by relatively gentle slopes, have fewer terraces. In the hilly areas of the Sichuan Basin and the Yunnan-Kweichou Plateau, terraces are primarily constructed by humans in the long-term process of adapting to nature through the reshaping of mountainous landscapes (Zhang et al., 2008; Duan et al., 2020). This process has also

270



fostered unique cultural and social practices associated with terraces (Zhan and Jin, 2015; Zhang et al., 2024). These regions face challenges such as limited cultivated land resources, steep slopes, and intense precipitation (Liu et al., 2014; Li et al., 2016; Wang and Dai, 2020). The construction of terraces not only acquires additional cultivable land but also optimizes water resource utilization and reduces soil erosion (Wei et al., 2017). In recent years, the Chinese Land Consolidation projects and the Well-facilitated Farmland projects have prioritized slope-to-terrace conversion as the primary land consolidation strategy in mountainous regions (Tang et al., 2019), significantly increasing the terrace area in southwestern China. In the Loess Plateau, terraces are mainly constructed for SWC and ecological restoration. Natural factors such as fragmented mountainous terrain, loose soil, and intense rainfall, coupled with human activities like deforestation, overgrazing, and cultivation on steep slope, have made the Loess Plateau one of China's most severely eroded regions (Wang et al., 2010; Liang et al., 2015). Over the past few decades, large-scale programs such as Grain-for-Green and terrace construction initiatives have been implemented to combat soil and water loss (Fu et al., 2017). Most terraces in the Loess Plateau are dryland terraces, predominantly located in Gansu, Ningxia, Shanxi, and Shaanxi. In northeast China, cropland has long slope lengths but gentle slope degrees (Liu et al., 2020a), resulting in fewer terraces being built. In contrast, in the hilly regions of central and southeastern China, terraces have also been constructed despite gentler slopes. Unlike the Sichuan Basin, Loess Plateau, and Yunnan-Guizhou Plateau, where terraces serve as a necessity for managing steep terrain, the primary motivation in these areas is to expand the cropland for the cultivation of economic crops such as tea and fruit trees (Adgo et al., 2013).

4.2 Soil erosion and conservation of terraces

The soil conservation benefits of terraces in China perform well generally. The Yunnan-Kweichou Plateau, the Sichuan Basin and the Loess Plateau are the regions with the best soil conservation benefits of terraces. In the past, the soil conservation benefits of terraces were often overlooked in large-scale soil erosion assessments due to the difficulty in obtaining spatial distribution of terraces. The soil erosion modulus of cropland was estimated as potential erosion under conditions without SWC, leading to an overestimation of the erosion modulus compared to assessments with conservation measures. For instance, the assessment of soil erosion on Chinese cropland by Wang et al. (2021). Indeed, soil erosion assessments in Europe, Australia, and Africa have similarly failed to consider the impact of terraces (Gobin et al., 2004; Teng et al., 2016; Salhi et al., 2025). Although the latest soil erosion assessment in Europe has considered terraces, it often extrapolates the survey results from sampled terraces to a regional scale through spatial interpolation, resulting in significant uncertainties in the localized erosion assessment of cropland (Panagos et al., 2015). Therefore, accurate and detailed information on terrace extent is crucial for the accurate assessment of soil erosion.

According to our estimation, the soil erosion of the Loess Plateau accounts for only 10.95% of the total cropland erosion in China, indicating that the SWC measures previously implemented have achieved good governance. The focus of SWC efforts in the Loess Plateau could transition from extensive engineering projects to tillage practice and biological practice aimed at increasing crop yields. Instead, cropland in northeastern China, characterized by long slope lengths but gentle slope



degrees, experiences severe erosion, representing 20.63% of the total cropland erosion. In southwest China, although the
305 proportion of terraces exceeds 70%, the widely distributed sloping cropland results in an average soil erosion modulus that
exceeds $15 \text{ t}\cdot\text{ha}^{-1}\cdot\text{y}^{-1}$, contributing 31.27% of the total cropland erosion. The effect of SWC engineering measures in
northeast and southwest China still has great room for improvement, which should be key areas of focus in future
conservation efforts. Although Hebei, Henan and Shandong feature gentle terrain, the extensive cropland and high planting
intensity contribute to soil erosion, which accounts for 15.48% of the total cropland erosion and warrants attention. From a
310 temporal changes perspective, with economic development and the implementation of national policies, China's SWC
measures have consistently shown an increasing trend, which no doubt decreased soil erosion and increased grain production
(Li et al., 2014; Liu et al., 2020a).

4.3 Limitations and prospects

The average OA for classifying terraces and non-terraces is 91.90%, with an average F1 score of 85.92%, indicating
315 satisfactory overall performance. However, for specific terrace types, the UA and PA of level terraces and zig terraces were
lower, resulting in relatively lower overall accuracy metrics such as OA and KA (Pontius, 2000). In mountainous and hilly
areas, the surface width of a level terrace generally ranges from 5 to 15 m, while the surface width of zig terrace is between
1.0 and 1.5 m, with both types having more sporadic (Duan et al., 2020). In this study, the 30 m resolution remote sensing
image effectively identified level terraces and zig terraces only when they exhibited concentrated and continuous
320 distributions, making it challenging to detect fragmented patches. In terms of UA, the probability of misclassification of
level terraces and zig terraces was low, indicating that the identified level terraces and zig terraces are reliable. However,
their numbers were underestimated. In 2000, the UA and PA of the slope-separated terrace were lower (Li et al., 2021). This
is mainly due to their small areas, which led to lower classification accuracy. To improve classification accuracy and
efficiency, cropland data from GlobeLand30 (2000-2020) was used as the basis for terrace identification. Inevitably, the
325 accuracy of GlobeLand30's cropland data impacts the terrace mapping process, as errors in cropland data propagate into the
terrace maps. Despite this limitation, the resulting error is deemed acceptable for terrace identification at the national scale
(Cao et al., 2021). Future studies could address these limitations by employing high-resolution remote sensing imagery,
which would enable improved detection of subpixel terrace distributions. Additionally, using more accurate cropland
datasets could further reduce errors and improve the overall accuracy of terrace mapping.

330 5 Data availability

The Landsat imagery and SRTM DEM data were acquired from the Google Earth Engine. The GlobeLand30 can be
downloaded from the National Geomatics Center of China. The 1 km spatial resolution SWCTMD (calculated from the 30 m
resolution SWCTMD) can be accessed at <https://doi.org/10.11888/Terre.tpd.302400> (Duan, 2025). The 30 m resolution
SWCTMD will be available after publication.



335 6 Conclusions

This study developed the first SWC terrace measures dataset for China with a fine classification system at a spatial resolution of 30 m. The dataset includes data for each decade from 2000 to 2020. It was generated by combining the full archive of Landsat imagery, digital elevation model, and nationally scaled samples of manual visualization, using a two-stage random forest classification on the GEE platform. The average OA and average F1 score for identifying terraces and
340 non-terraces were 91.90 % and 85.92%, respectively. For different terrace types, the average OA and average F1 score were 83.50% and 52.14%, respectively.

Compared to existing terrace datasets, the newly developed dataset provides more comprehensive coverage, especially in identifying zig terraces in southeastern China. The dataset reveals that, terraces are primarily distributed in the Loess Plateau, Southwest China, and Southeast China. From 2000 to 2020, the total terrace areas expanded by 96,038.16 km², with level
345 terraces increasing by 2,275.26 km², slope terraces by 86,186.26 km², slope-separated terraces by 6,040.36 km², and zig terraces by 1,536.28 km². Terrace expansion was mainly concentrated in the Loess Plateau and southwest and Southeast regions of China, while the terrace decrease was mainly observed around urban areas.

Terraces in China are estimated to have reduced soil erosion on cropland by approximately 818 million tons. Further analysis highlighted benefits of SWC in the Yunnan-Guizhou Plateau and Loess Plateau are the best. The terrace dataset, with its
350 detailed classification system is expected to provide a cornerstone for national and regional soil erosion assessment and prediction, SWC planning, and evaluations of various ecosystem services related to terraces.

Author contributions

XD conceived and designed the study. EZ conducted the construction of the dataset and wrote the manuscript. EZ, HW, BD collected the data. CL provided the technical support. SW, HL, XY and YL provided assistance with the data analysis. YC
355 and XD edited and revised the manuscript.

Competing interests

The contact author has declared that none of the authors has any competing interests.

Acknowledgments

We express our great gratitude to the free access to the Landsat data provided by the USGS, SRTM DEM provided by the
360 National Aeronautics and Space Administration (NASA)/USGS/Jet Propulsion Laboratory (JPL), GlobeLand30 provided by the National Geomatics Center of China, and the cloud computing power provided by GEE.



Financial support

This research was supported by the National Natural Science Foundation Project of China (grant no. U24A20581) and the National Key Research and Development Program of China (grant no. 2023YFD1901201).

365 References

- Adgo, E., Teshome, A., and Mati, B.: Impacts of long-term soil and water conservation on agricultural productivity: The case of Anjenie watershed, Ethiopia, *Agric. Water Manage.*, 117, 55-61, <https://doi.org/10.1016/j.agwat.2012.10.026>, 2013.
- Arnáez, J., Lana-Renault, N., Lasanta, T., Ruiz-Flaño, P., and Castroviejo, J.: Effects of farming terraces on hydrological and geomorphological processes. A review, *Catena*, 128, 122-134, <https://doi.org/10.1016/j.catena.2015.01.021>, 2015.
- 370 Cao, B., Yu, L., Naipal, V., Ciais, P., Li, W., Zhao, Y., Wei, W., Chen, D., Liu, Z., and Gong, P.: A 30 m terrace mapping in China using Landsat 8 imagery and digital elevation model based on the Google Earth Engine, *Earth Syst. Sci. Data*, 13, 2437-2456, <https://doi.org/10.5194/essd-13-2437-2021>, 2021.
- Chen, D., Wei, W., and Chen, L.: Effects of terracing practices on water erosion control in China: A meta-analysis, *Earth Sci. Rev.*, 173, 109-121, <https://doi.org/10.1016/j.earscirev.2017.08.007>, 2017.
- 375 Chen, D., Wei, W., and Chen, L.: How can terracing impact on soil moisture variation in China? A meta-analysis, *Agric. Water Manage.*, 227, 105849, <https://doi.org/10.1016/j.agwat.2019.105849>, 2020.
- Chen, J., Chen, J., Liao, A., Cao, X., Chen, L., Chen, X., He, C., Han, G., Peng, S., Lu, M., Zhang, W., Tong, X., and Mills, J.: Global land cover mapping at 30m resolution: A POK-based operational approach, *ISPRS J. Photogramm. Remote Sens.*, 103, 7-27, <https://doi.org/10.1016/j.isprsjprs.2014.09.002>, 2015.
- 380 Chen, R., Yin, B., Yang, W., Li, J., Li, Z., Zhang, Y., and Chen, J.: Mapping the successional stages of biological soil crusts at 3-m resolution in the Gurbantunggut Desert, China through hydration-induced spectral response, *Remote Sens. Environ.*, 310, 114230, <https://doi.org/10.1016/j.rse.2024.114230>, 2024.
- Deng, C., Zhang, G., Liu, Y., Nie, X., Li, Z., Liu, J., and Zhu, D.: Advantages and disadvantages of terracing: A comprehensive review, *Int. Soil Water Conserv. Res.*, 9, 344-359, <https://doi.org/10.1016/j.iswcr.2021.03.002>, 2021.
- 385 Dong, Y., Chang, H.-C., Chen, W., Zhang, K., and Feng, R.: Accuracy assessment of GDEM, SRTM, and DLR-SRTM in Northeastern China, *Geocarto Int.*, 30, 779-792, <https://doi.org/10.1080/10106049.2014.985744>, 2015.
- Duan, M., Song, X., Liu, X., Cui, D., and Zhang, X.: Mapping the soil types combining multi-temporal remote sensing data with texture features, *Comput. Electron. Agric.*, 200, 107230, <https://doi.org/10.1016/j.compag.2022.107230>, 2022.
- Duan, M., Song, X., Li, Z., Zhang, X., Ding, X., and Cui, D.: Identifying soil groups and selecting a high-accuracy classification method based on multi-textural features with optimal window sizes using remote sensing images, *Ecol. Inf.*, 81, 102563, <https://doi.org/10.1016/j.ecoinf.2024.102563>, 2024.
- 390



- Duan, X., Bai, Z., Rong, L., Li, Y., Ding, J., Tao, Y., Li, J., Li, J., and Wang, W.: Investigation method for regional soil erosion based on the Chinese Soil Loss Equation and high-resolution spatial data: Case study on the mountainous Yunnan Province, China, *Catena*, 184, 104237, <https://doi.org/10.1016/j.catena.2019.104237>, 2020.
- 395 Farr, T. G., Rosen, P. A., Caro, E., Crippen, R., Duren, R., Hensley, S., Kobrick, M., Paller, M., Rodriguez, E., Roth, L., Seal, D., Shaffer, S., Shimada, J., Umland, J., Werner, M., Oskin, M., Burbank, D., and Alsdorf, D.: The Shuttle Radar Topography Mission, *Rev. Geophys.*, 45, <https://doi.org/10.1029/2005RG000183>, 2007.
- Feng, W., Yang, Y., Zhao, Y., Di, B., and Ma, C.: The Implementation Effects of a Nationwide Sloping Farmland Soil Erosion Control Project in China, *J. Resour. Ecol.*, 8, 341-351, <https://doi.org/10.5814/j.issn.1674-764x.2017.04.005>, 2017.
- 400 Fu, B., Wang, S., Liu, Y., Liu, J., Liang, W., and Miao, C.: Hydrogeomorphic Ecosystem Responses to Natural and Anthropogenic Changes in the Loess Plateau of China, *Annu. Rev. Earth Planet. Sci.*, 45, 223-243, <https://doi.org/10.1146/annurev-earth-063016-020552>, 2017.
- Gobin, A., Jones, R., Kirkby, M., Campling, P., Govers, G., Kosmas, C., and Gentile, A. R.: Indicators for pan-European assessment and monitoring of soil erosion by water, *Environmental Science & Policy*, 7, 25-38, <https://doi.org/10.1016/j.envsci.2003.09.004>, 2004.
- 405 Gong, P., Liu, H., Zhang, M., Li, C., Wang, J., Huang, H., Clinton, N., Ji, L., Li, W., Bai, Y., Chen, B., Xu, B., Zhu, Z., Yuan, C., Ping Suen, H., Guo, J., Xu, N., Li, W., Zhao, Y., Yang, J., Yu, C., Wang, X., Fu, H., Yu, L., Dronova, I., Hui, F., Cheng, X., Shi, X., Xiao, F., Liu, Q., and Song, L.: Stable classification with limited sample: transferring a 30-m resolution sample set collected in 2015 to mapping 10-m resolution global land cover in 2017, *Sci. Bull.*, 64, 370-373, <https://doi.org/10.1016/j.scib.2019.03.002>, 2019.
- 410 Gong, P., Chen, B., Li, X., Liu, H., Wang, J., Bai, Y., Chen, J., Chen, X., Fang, L., Feng, S., Feng, Y., Gong, Y., Gu, H., Huang, H., Huang, X., Jiao, H., Kang, Y., Lei, G., Li, A., Li, X., Li, X., Li, Y., Li, Z., Li, Z., Liu, C., Liu, C., Liu, M., Liu, S., Mao, W., Miao, C., Ni, H., Pan, Q., Qi, S., Ren, Z., Shan, Z., Shen, S., Shi, M., Song, Y., Su, M., Ping Suen, H., Sun, B., Sun, F., Sun, J., Sun, L., Sun, W., Tian, T., Tong, X., Tseng, Y., Tu, Y., Wang, H., Wang, L., Wang, X., Wang, Z., Wu, T.,
- 415 Xie, Y., Yang, J., Yang, J., Yuan, M., Yue, W., Zeng, H., Zhang, K., Zhang, N., Zhang, T., Zhang, Y., Zhao, F., Zheng, Y., Zhou, Q., Clinton, N., Zhu, Z., and Xu, B.: Mapping essential urban land use categories in China (EULUC-China): preliminary results for 2018, *Sci. Bull.*, 65, 182-187, <https://doi.org/10.1016/j.scib.2019.12.007>, 2020.
- He, Y., Lee, E., and Warner, T. A.: A time series of annual land use and land cover maps of China from 1982 to 2013 generated using AVHRR GIMMS NDVI3g data, *Remote Sens. Environ.*, 199, 201-217, <https://doi.org/10.1016/j.rse.2017.07.010>, 2017.
- 420 Hirayama, H., Sharma, R. C., Tomita, M., and Hara, K.: Evaluating multiple classifier system for the reduction of salt-and-pepper noise in the classification of very-high-resolution satellite images, *Int. J. Remote Sens.*, 40, 2542-2557, <https://doi.org/10.1080/01431161.2018.1528400>, 2019.
- Hou, Q., Wang, F., and Yan, L.: Extraction of color image texture feature based on gray-level co-occurrence matrix, *Remote Sensing For Land & Resources*, 25, 26-32, 2013.
- 425



- Li, J., He, H., Zeng, Q., Chen, L., and Sun, R.: A Chinese soil conservation dataset preventing soil water erosion from 1992 to 2019, *Sci. Data*, 10, 319, <https://doi.org/10.1038/s41597-023-02246-4>, 2023.
- Li, K., Yang, J., Wang, J., Wang, Z., Zeng, Y., Borrelli, P., Hubacek, K., Hu, Y., Xu, B., Fang, N., Zeng, C., Zhou, Z., and Shi, Z.: Human-altered soil loss dominates nearly half of water erosion in China but surges in agriculture-intensive areas, *One Earth*, <https://doi.org/10.1016/j.oneear.2024.09.001>, 2024.
- 430 Li, Y., Liu, C., Zhang, J., Zhang, P., and Xue, Y.: Monitoring Spatial and Temporal Patterns of Rubber Plantation Dynamics Using Time-Series Landsat Images and Google Earth Engine, *IEEE J. Sel. Top. Appl. Earth Obs. Remote Sens.*, 14, 9450-9461, <https://doi.org/10.1109/JSTARS.2021.3110763>, 2021.
- Li, Y., Zhang, W., Ma, L., Wu, L., Shen, J., Davies, W. J., Oenema, O., Zhang, F., and Dou, Z.: An analysis of China's grain production: looking back and looking forward, *Food and Energy Security*, 3, 19-32, <https://doi.org/10.1002/fes3.41>, 2014.
- 435 Li, Z., Xu, X., Yu, B., Xu, C., Liu, M., and Wang, K.: Quantifying the impacts of climate and human activities on water and sediment discharge in a karst region of southwest China, *J. Hydrol.*, 542, 836-849, <https://doi.org/10.1016/j.jhydrol.2016.09.049>, 2016.
- Liang, W., Bai, D., Wang, F., Fu, B., Yan, J., Wang, S., Yang, Y., Long, D., and Feng, M.: Quantifying the impacts of climate change and ecological restoration on streamflow changes based on a Budyko hydrological model in China's Loess Plateau, *Water Resour. Res.*, 51, 6500-6519, <https://doi.org/10.1002/2014WR016589>, 2015.
- 440 Liu, B., Liu, Y., Zhang, K., and Xie, Y.: Classification for Soil Conservation Practices in China, *J. Soil Water Conserv.*, 27, 80-84, <https://doi.org/10.13870/j.cnki.stbcbx.2013.02.025>, 2013a.
- Liu, B., Xie, Y., Li, Z., Liang, Y., Zhang, W., Fu, S., Yin, S., Wei, X., Zhang, K., Wang, Z., Liu, Y., Zhao, Y., and Guo, Q.: The assessment of soil loss by water erosion in China, *Int. Soil Water Conserv. Res.*, 8, 430-439, <https://doi.org/10.1016/j.iswcr.2020.07.002>, 2020a.
- 445 Liu, D., Chen, N., Zhang, X., Wang, C., and Du, W.: Annual large-scale urban land mapping based on Landsat time series in Google Earth Engine and OpenStreetMap data: A case study in the middle Yangtze River basin, *ISPRS J. Photogramm. Remote Sens.*, 159, 337-351, <https://doi.org/10.1016/j.isprsjprs.2019.11.021>, 2020b.
- 450 Liu, J., Zhang, Z., Xu, X., Kuang, W., Zhou, W., Zhang, S., Li, R., Yan, C., Yu, D., Wu, S., and Jiang, N.: Spatial patterns and driving forces of land use change in China during the early 21st century, *J. Geogr. Sci.*, 20, 483-494, <https://doi.org/10.1007/s11442-010-0483-4>, 2010.
- Liu, M., Xu, X., Sun, A. Y., Wang, K., Liu, W., and Zhang, X.: Is southwestern China experiencing more frequent precipitation extremes?, *Environ. Res. Lett.*, 9, 064002, <https://doi.org/10.1088/1748-9326/9/6/064002>, 2014.
- 455 Liu, S. L., Dong, Y. H., Li, D., Liu, Q., Wang, J., and Zhang, X. L.: Effects of different terrace protection measures in a sloping land consolidation project targeting soil erosion at the slope scale, *Ecol. Eng.*, 53, 46-53, <https://doi.org/10.1016/j.ecoleng.2012.12.001>, 2013b.
- Liu, X., Xin, L., and Lu, Y.: National scale assessment of the soil erosion and conservation function of terraces in China, *Ecol. Indic.*, 129, 107940, <https://doi.org/10.1016/j.ecolind.2021.107940>, 2021.



- 460 Londero, A. L., Minella, J. P. G., Deuschle, D., Schneider, F. J. A., Boeni, M., and Merten, G. H.: Impact of broad-based terraces on water and sediment losses in no-till (paired zero-order) catchments in southern Brazil, *J. Soils Sediments*, 18, 1159-1175, <https://doi.org/10.1007/s11368-017-1894-y>, 2018.
- Lu, M., Wu, W., Zhang, L., Liao, A., Peng, S., and Tang, H.: A comparative analysis of five global cropland datasets in China, *Sci. China Earth Sci.*, 59, 2307-2317, <https://doi.org/10.1007/s11430-016-5327-3>, 2016.
- 465 Lu, Y., Li, X., Xin, L., Song, H., and Wang, X.: Mapping the terraces on the Loess Plateau based on a deep learning-based model at 1.89 m resolution, *Sci. Data*, 10, 115, <https://doi.org/10.1038/s41597-023-02005-5>, 2023.
- Masek, J. G., Vermote, E. F., Saleous, N. E., Wolfe, R., Hall, F. G., Huemmrich, K. F., Feng, G., Kutler, J., and Teng-Kui, L.: A Landsat surface reflectance dataset for North America, 1990-2000, *IEEE Geosci. Remote Sens. Lett.*, 3, 68-72, <https://doi.org/10.1109/LGRS.2005.857030>, 2006.
- 470 Maskell, G., Chemura, A., Nguyen, H., Gornott, C., and Mondal, P.: Integration of Sentinel optical and radar data for mapping smallholder coffee production systems in Vietnam, *Remote Sens. Environ.*, 266, 112709, <https://doi.org/10.1016/j.rse.2021.112709>, 2021.
- Oliveira, J. R. S. d., Pruski, F. F., Silva, J. M. A. d., and Siya, D. P. d.: Comparative analysis of the performance of mixed terraces and level and graded terraces, *Acta Sci.-Agron.*, 34, 351-357, <https://doi.org/10.4025/actasciagr.v34i4.14755>, 2012.
- 475 Panagos, P., Borrelli, P., Poesen, J., Ballabio, C., Lugato, E., Meusburger, K., Montanarella, L., and Alewell, C.: The new assessment of soil loss by water erosion in Europe, *Environmental Science & Policy*, 54, 438-447, <https://doi.org/10.1016/j.envsci.2015.08.012>, 2015.
- Pontius, R. G.: Quantification error versus location error in comparison of categorical maps, *Photogramm. Eng. Remote Sens.*, 66, 1011-1016, 2000.
- 480 Renard, K. G., Foster, G. A., Weesies, D. K. M., and Yoder, D. C.: Predicting soil erosion by water: a guide to conservation planning with the Revised Universal Soil Loss Equation (RUSLE), *Agriculture Handbook*, United States Department of Agriculture, Washington D. C. 1997.
- Rodriguez-Galiano, V. F., Chica-Olmo, M., Abarca-Hernandez, F., Atkinson, P. M., and Jeganathan, C.: Random Forest classification of Mediterranean land cover using multi-seasonal imagery and multi-seasonal texture, *Remote Sens. Environ.*, 121, 93-107, <https://doi.org/10.1016/j.rse.2011.12.003>, 2012a.
- 485 Rodriguez-Galiano, V. F., Ghimire, B., Rogan, J., Chica-Olmo, M., and Rigol-Sanchez, J. P.: An assessment of the effectiveness of a random forest classifier for land-cover classification, *ISPRS J. Photogramm. Remote Sens.*, 67, 93-104, <https://doi.org/10.1016/j.isprsjprs.2011.11.002>, 2012b.
- Roy, D. P., Kovalsky, V., Zhang, H. K., Vermote, E. F., Yan, L., Kumar, S. S., and Egorov, A.: Characterization of Landsat-7 to Landsat-8 reflective wavelength and normalized difference vegetation index continuity, *Remote Sens. Environ.*, 185, 57-70, <https://doi.org/10.1016/j.rse.2015.12.024>, 2016.
- 490 Salhi, A., Benabdelouahab, S., and Heggy, E.: Soil erosion susceptibility maps and raster dataset for the hydrological basins of North Africa, *Sci. Data*, 12, 65, [10.1038/s41597-025-04406-0](https://doi.org/10.1038/s41597-025-04406-0), 2025.



- 495 Tang, G., Li, F., and Liu, X.: Extraction of slope terrain factors, in: Course of digital elevation model, 3rd Edition, Science Press, Beijing, China, 134-156, 2016.
- Tang, H., Yun, W., Liu, W., and Sang, L.: Structural changes in the development of China's farmland consolidation in 1998–2017: Changing ideas and future framework, *Land Use Policy*, 89, 104212, <https://doi.org/10.1016/j.landusepol.2019.104212>, 2019.
- 500 Teng, H., Viscarra Rossel, R. A., Shi, Z., Behrens, T., Chappell, A., and Bui, E.: Assimilating satellite imagery and visible–near infrared spectroscopy to model and map soil loss by water erosion in Australia, *Environmental Modelling & Software*, 77, 156-167, <https://doi.org/10.1016/j.envsoft.2015.11.024>, 2016.
- Tu, Y., Wu, S., Chen, B., Weng, Q., Bai, Y., Yang, J., Yu, L., and Xu, B.: A 30 m annual cropland dataset of China from 1986 to 2021, *Earth Syst. Sci. Data*, 16, 2297-2316, <https://doi.org/10.5194/essd-16-2297-2024>, 2024.
- 505 Wang, T., Wu, J., Kou, X., Oliver, C., Mou, P., and Ge, J.: Ecologically asynchronous agricultural practice erodes sustainability of the Loess Plateau of China, *Ecol. Appl.*, 20, 1126-1135, <https://doi.org/10.1890/09-0229.1>, 2010.
- Wang, Y. and Dai, E.: Spatial-temporal changes in ecosystem services and the trade-off relationship in mountain regions: A case study of Hengduan Mountain region in Southwest China, *J. Cleaner Prod.*, 264, 121573, <https://doi.org/10.1016/j.jclepro.2020.121573>, 2020.
- 510 Wang, Z., Zeng, Y., Li, C., Yan, H., Yu, S., Wang, L., and Shi, Z.: Telecoupling cropland soil erosion with distant drivers within China, *Journal of Environmental Management*, 288, 112395, <https://doi.org/10.1016/j.jenvman.2021.112395>, 2021.
- Wei, W., Pan, D., and Yang, Y.: Effects of terracing measures on water retention of pinus *Tabulaeformis* forest in the dryland loess hilly region of China, *Agric. For. Meteorol.*, 308-309, 108544, <https://doi.org/10.1016/j.agrformet.2021.108544>, 2021.
- 515 Wei, Z., Han, Y., Li, M., Yang, K., Yang, Y., Luo, Y., and Ong, S.-H.: A Small UAV Based Multi-Temporal Image Registration for Dynamic Agricultural Terrace Monitoring, <https://doi.org/10.3390/rs9090904>, 2017.
- Wickama, J., Okoba, B., and Sterk, G.: Effectiveness of sustainable land management measures in West Usambara highlands, Tanzania, *Catena*, 118, 91-102, <https://doi.org/10.1016/j.catena.2014.01.013>, 2014.
- Wischmeier, W. H. and Smith, D. D.: Predicting rainfall erosion losses: a guide to conservation planning, Science and Education Administration, Washington D. C., America, 1978.
- 520 Yang, J. and Huang, X.: The 30 m annual land cover dataset and its dynamics in China from 1990 to 2019, *Earth Syst. Sci. Data*, 13, 3907-3925, <https://doi.org/10.5194/essd-13-3907-2021>, 2021.
- Yu, L., Wang, J., and Gong, P.: Improving 30 m global land-cover map FROM-GLC with time series MODIS and auxiliary data sets: a segmentation-based approach, *Int. J. Remote Sens.*, 34, 5851-5867, <https://doi.org/10.1080/01431161.2013.798055>, 2013.
- 525 Zhan, G. and Jin, Z.: Hani Rice Terraces of Honghe - The Harmonious Landscape of Nature and Humans, *Landscape Res.*, 40, 655-667, <https://doi.org/10.1080/01426397.2015.1060299>, 2015.



- Zhang, J. H., Su, Z. A., and Liu, G. C.: Effects of terracing and agroforestry on soil and water loss in hilly areas of the Sichuan Basin, China, *J. Mountain Sci.*, 5, 241-248, <https://doi.org/10.1007/s11629-008-0189-6>, 2008.
- 530 Zhang, X., Liu, L., Chen, X., Gao, Y., Xie, S., and Mi, J.: GLC_FCS30: global land-cover product with fine classification system at 30 m using time-series Landsat imagery, *Earth Syst. Sci. Data*, 13, 2753-2776, <https://doi.org/10.5194/essd-13-2753-2021>, 2021.
- Zhang, Y., Zhang, A., and Ma, Y.: An integrated mechanism and challenges of mountainous sustainable development: A review of Hani Terraces, China, *Sustainable Dev.*, 32, 101-118, <https://doi.org/10.1002/sd.2651>, 2024.
- 535 Zhang, Y., Shi, M., Zhao, X., Wang, X., Luo, Z., and Zhao, y.: Methods for automatic identification and extraction of terraces from high spatial resolution satellite data (China-GF-1), *Int. Soil Water Conserv. Res.*, 5, 17-25, <https://doi.org/10.1016/j.iswcr.2017.02.002>, 2017.
- Zhang, Y., Tian, P., Yang, L., Zhao, G., Mu, X., Wang, B., Du, P., Gao, P., and Sun, W.: Relationship between sediment load and climate extremes in the major Chinese rivers, *J. Hydrol.*, 617, 128962, <https://doi.org/10.1016/j.jhydrol.2022.128962>, 2023.
- 540 Zhu, Z. and Woodcock, C. E.: Object-based cloud and cloud shadow detection in Landsat imagery, *Remote Sens. Environ.*, 118, 83-94, <https://doi.org/10.1016/j.rse.2011.10.028>, 2012.